JOURNAL GEOLOGICAL SOCIETY OF INDIA
Vol.97, January 2021, pp.9-20

Characteristics of the Seismic Clusters Bounding the Ramu-Markham Fault Zone, Eastern Papua New Guinea

George Noho[1], Manoj Mukhopadhyay[1], Basab Mukhopadhyay[2*] and Diptansu Sengupta[2]

[1]Department of Applied Physics, Papua New Guinea University of Technology, Lae, 411 Morobe Province, Paua New Guinea.
[2]Geological Survey of India, #29, J.L. Nehru Road, Kolkata - 700 016, India
E-mail: *basabmukhopadhyay@gmail.com*; giinoho@gmail.com; manoj.mukhopadhyay@pnguot.ac.pg; diptansu.sengupta@gmail.com*

ABSTRACT

The regionally extensive Ramu-Markham-Fault-Zone (RMFZ) in Papua-New-Guinea (PNG) passes through the seismically-active hinterland of the Bismarck subduction zone in SW-Pacific. The seismicity map for 400km segment of RMFZ shows that higher magnitude earthquakes mainly originate in four spatial clusters (I-IV), asymmetrically disposed from in-land to offshore on either side of RMFZ. The cluster III have produced the 2019 Bulolo-earthquake (Mw 7.1). The spatial and temporal characters for all four seismic clusters was estimated by: (i) b-value based on maximum-likelihood method; (ii) expected maximum magnitude (Mw) by Gumbel extreme value statistics and surface rupture length; and (iii) the Hurst coefficient (K) and Hurst plot. Hurst plots on sequential seismic moments in the clusters illustrate an alternating positive and negative sloping moment-release pattern over progressive time-period that corresponds to low and high b-values respectively. The regional stress pattern on north and south of RMFZ and for four seismic clusters are analysed by inversion of CMT focal-mechanism data. The result unravels a significant change in regional stress pattern across the RMFZ: (i) a pure-compressive stress regime corresponding to clusters I and II in the 'PNG Highlands' that gradually changes to transpressive in the off-shore cluster IV along north of RMFZ, and (ii) the regional stress pattern for earthquakes south of RMFZ including cluster III shows absence of any particular stress orientation and causative faults are randomly oriented. This leads to the presentation that RMFZ is a deep penetrative fault, rather than a crustal ramp fault restricted to 11-18km depth as advocated in literature.

INTRODUCTION

The "Lae Seismic Zone" belonging to the Markham valley located in eastern PNG is of much geodynamic interest due to its close proximity to the offshore subduction zone under the south Bismarck Sea in SW Pacific. The region is prone to seismicity as evidenced by occurrence of numerous earthquakes; an unauthentic estimate puts this at 300 earthquakes annually, most of which are however of smaller magnitude. Here the recorded land deformation is primarily an outcome of the convergence of the two large plates: Australian and Pacific plates, within which, the New Guinea Highland and south Bismarck microplates are trapped, thus forming a complex convergent boundary (Fig. 1).

Measurements from geodetic network, accelerograph and seismograph network in PNG have helped the seismologists to draw conclusion that the Australian and Pacific continental plates, drifting NE and SW respectively, are colliding at a rate of 55 mm/yr. giving rise to smaller microplates in which the island of PNG is resting. RMFZ shows a convergence normal to the fault line (Abers and McCaffrey 1994; Stevens et al. 1998; Tregoning et al. 1999) and the motion increases from a few mm/yr. in the NW to 61 mm/yr. to the SE (Wallace et al. 2004) showing clockwise rotation of the plate. As a result of the subduction process, the land areas to the north of Lae is experiencing noticeable uplift, with an estimated rate of 0.8 – 2.1 mm/yr. along the southern flanks of the Finisterre range (Stanaway et al. 2009).

The regional seismicity studies so far published, have provided ample evidences that the areas to the north and south of RMFZ are prone to high level of seismicity. The areas to the north of RMFZ show, in particular, visible land deformation. The objectives of the present study are the followings: (a) to investigate the nature of regional and clustered seismicity in eastern part of PNG in correspondence to RMFZ, (b) to study the seismic characteristics and parameters for the four visible seismic clusters identified on either side of RMFZ, (c) to study the prevalent stress regime affecting the seismic clusters and their variations in the study area, and (d) to present an initial analysis on seismic hazard potentiality based on the available data by using Gumbel extreme value statistics and surface rupture length (SRL).

SOME THEORETICAL CONSIDERATION FOR SUBSEQUENT ANALYSIS

The conversion of earthquake magnitude (Mb) to Moment magnitude (Mw), is carried out by the conversion formula developed by Scordillis (2006):

$$Mw = 0.85(\pm 0.04)\ mb + 1.03(\pm 0.23),\ \text{for}\ 3.5 \leq mb \geq 6.2) \quad (1)$$

For calculating the seismic-moment M_0, in dyne-cm, for individual earthquake event, the equation developed by Hanks and Kanamori (1979), has been used

$$\log M_0 = 1.5Mw + 10.05 \quad (2).$$

Similarly, for calculating the *b*-value by Maximum Likelihood Method (MLM), the equation developed by Aki (1965) is used as

$$b = (\text{Log}_{10}\, e) / (M_{av} - M_{min}) \quad (3),$$

where, M_{av} is the mean magnitude above the threshold M_{min}.

The standard deviation (∂b) of the error in *b*-value estimation is computed using the equation Shi and Bolt (1982) as:

$$\partial b = 2.3b^2 \sqrt{\Sigma_{i=1}^{n}(M_i - M_{av})^2/n(n-1)} \quad (4),$$

where M_i is the magnitude of individual earthquake, M_{av} is the mean magnitude and n is the number of events.

The theoretical background and equations used for calculation

0016-7622/2021-97-1-9/$ 1.00 © GEOL. SOC. INDIA | DOI: 10.1007/s12594-021-1621-6

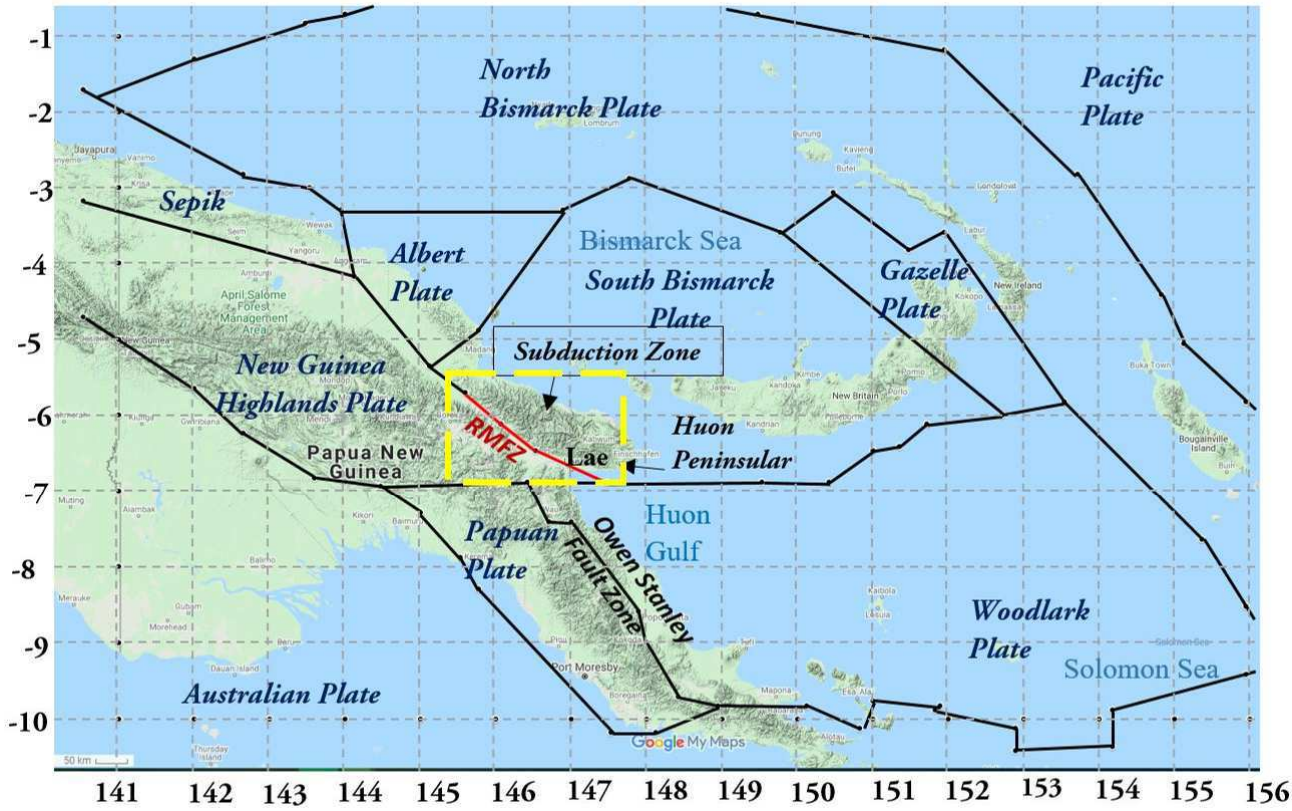

Fig.1. The Plate boundaries (source: Stanaway et al. 2014) and Ramu-Markham Fault Zone (RMFZ) in and around Papua New Guinea are marked. The present study area is demarcated by yellow coloured box.

of parameters in Gumbel's extreme value statistics is in Appendix 1.

The empirical relation between the expected Surface Rupture Length (SRL) and the magnitude of the earthquake (M) developed by Wells and Coppersmith (1994) and valid for reverse faulting in inter-plate tectonic region is

$$M = 5.08 + 1.16 \log SRL \quad (5).$$

The maximum displacement (MD) in meter for an earthquake for given magnitude M is calculated as

$$M = 6.69 + 0.74 \log MD \quad (6),$$

Wells and Coppersmith (1994).

SEISMICITY FOR EASTERN NEW GUINEA

Seismicity Map and Seismic Clusters

Here the USGS – NEIC Earthquake data for the eastern part of PNG located within the Latitudes 5 – 7.5° S and Longitudes 145-148° E, has been considered for the period 1964 – 2019. The earthquake magnitude (Mb) in NEIC catalogue is converted to a uniform scale, moment magnitude (Mw), by using equation 1 developed by Scordillis (2006). Further, "Hanks and Kanamori (1979) relationship" (also refer by McGuire 2004) is used to calculate the seismic-moment M_0 (dyne-cm), for individual earthquake event by equation 2. The conversion results obtained have been compared with the Mw and $Log_{10}(M_0)$ values given for the earthquakes in CMT catalogue of the area. The difference between Mw and $Log_{10}(M_0)$ values are statistically analysed; the difference in Mw has a mean 0.042 and standard deviation 0.138 whereas, the same for $Log_{10}(M_0)$ is 0.768 and 0.416 respectively. The above statistics indicate that both converted and actual data corroborated well, and converted earthquake data can be used for further analysis.

The earthquakes with Mw ≥ 2.8 are presented as a revised seismicity map for eastern PNG (Fig. 2), the earthquakes originate up to intermediate depths extending to 280 km. Figure 2 illustrates that the areas to the north and south of the Markham valley are active and the seismicity shows up in distinct spatial clusters separated by the RMFZ. Such visible spatial clusters, I to IV, on both sides of RMFZ are marked (Fig. 2). The magnitude and depth relations in these spatial clusters are random i.e., both smaller and larger magnitude earthquakes occur at shallow and deeper depths. Beach-balls of some of the larger earthquakes are plotted to show the kinematics over the entire terrain of study. The beach-balls show a highly compressive regime with majority of thrust and strike-slip earthquakes. The DEM for the region further suggests that the clustered seismicity originates underneath the Finisterre range rather than below the Markham valley proper, the latter is traversed by the RMFZ.

The clusters I through III are of variable appearance on surface. Seismic activity is further followed in SE-direction for about 100 km offshore from Lae, where one more such cluster, cluster IV, originates below the sea-floor maintaining this direction, in tectonic continuity of RMFZ (Fig.3a). Figure 3a displays all four seismic clusters which are considered as a manifestation of basic character of the regional seismicity, continuing from on-land into offshore, in close correspondence to RMFZ. Two topographic sections (sections 1 and 2, location on figure 3a) are drawn across the RMFZ to show the disposition of RMFZ in relation to surface topography, where RMFZ is represented as a high angle fault dipping towards north-east (Fig. 3b). An overall 3D distribution of seismicity in this sub-duction zone is shown to illustrate the downdip extension of seismicity along the subducting New Guinea Highlands plate with depth (Fig. 3c). An attempt has been made to show the subducting plate and overriding plate geometry along with its surface manifestation in 3D (Fig. 3d).

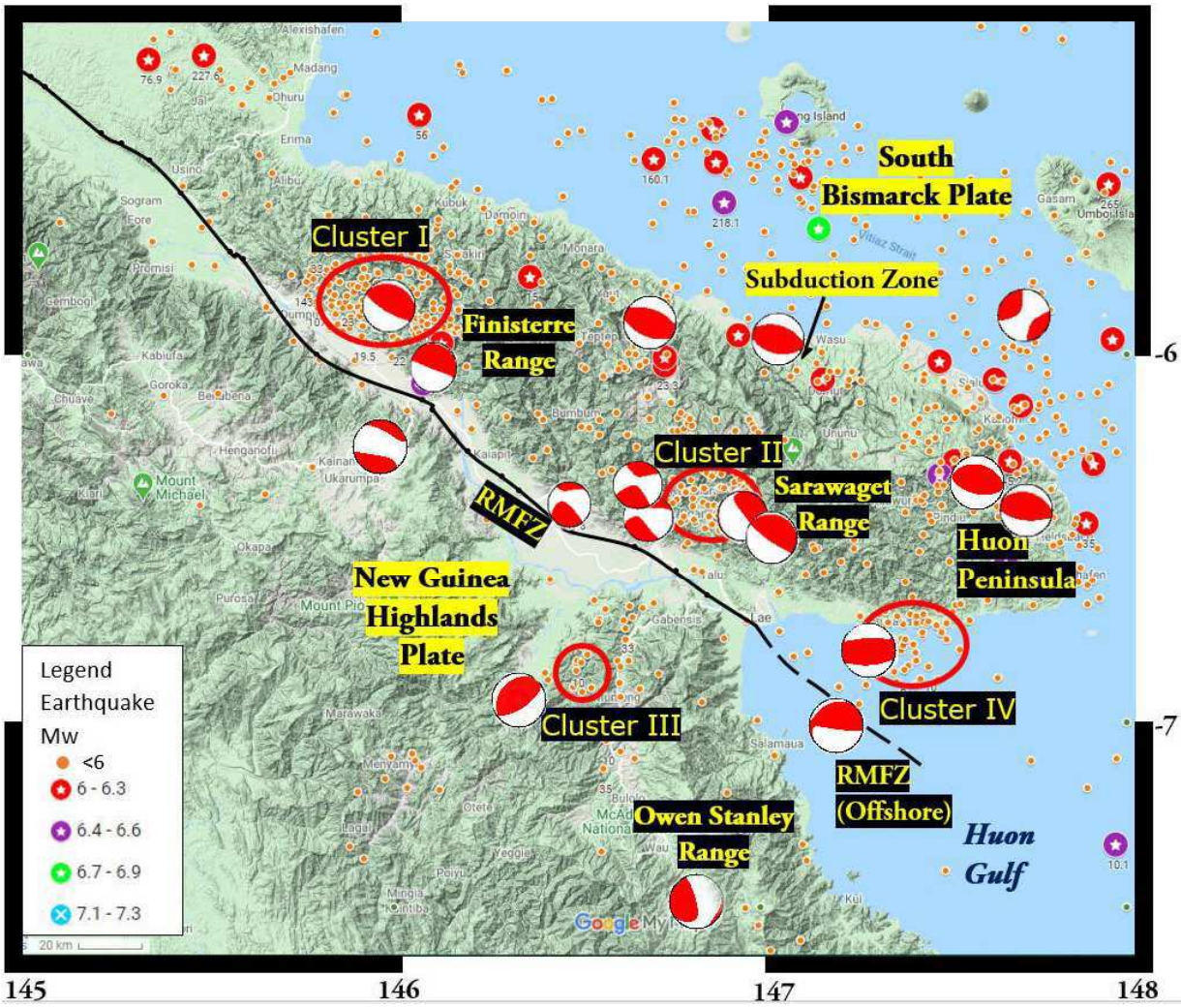

Fig. 2. Seismicity in the eastern Papua New Guinea, plot is centred at the port-city Lae. Earthquake distribution (Mw ≥ 2.8) is shown with magnitude classification as per index. Data period: 1964-2019, data source: USGS – NEIC. The subduction interface is marked. Dark thick line: Ramu Markham Fault Zone (RMFZ) on-land; offshore continuation is inferred. The zones for seismic clusters are identified. Beach-balls of some larger earthquakes are plotted to indicate overall kinematics of the region which is mostly compressional.

Depth – Magnitude Relationship in the Individual Seismic Clusters

3D-hypocentral plots are generated by the 'Teraplot software' using the USGS – NEIC seismicity data on earthquake magnitude (Mw) and focal depth in km corresponding to the clusters I through IV (Figs. 4 through 7). The following primary features are observed from the plots: (i) seismic zone contained in the clusters gives an appearance of a tornado with depth, (ii) the magnitude has no relations to the focal depth of the earthquakes as evident for all four clusters. Larger as well as smaller magnitude earthquakes occur at shallower to greater depths alike. For example, in cluster II an earthquake of magnitude 4.5 has occurred at a depth of approximately 209 km while there are earthquakes of the same magnitude that have occurred all over between 0 - 209 km (Fig. 5). Similarly, Fig. 4 shows earthquakes of cluster I where earthquake of magnitude 6.9 occurring at depths of 25.3 km, whereas there are earthquakes with smaller magnitudes that have occurred at greater depths. Comparable situation exists in cluster IV also (Fig. 7). The Bulolo earthquake of May 6th 2019, Mw 7.1, h = 146 km, occurred in cluster III (Fig. 6). It is one of the deep large earthquakes that struck the area.

Seismic Parameters in Earthquake Clusters

The seismic parameters examined here are: the earthquake numbers, magnitude range, main shocks, magnitude completeness (Mc), b-value with error estimates, are calculated for all four clusters (Table 1). Mc is estimated by MAXc approach, assuming self-similarity (Wiemer and Wyss 2000), while, *b*-value is calculated by maximum likelihood method (MLM) (Aki, 1965) using equation 3. The error in *b*-value estimation is computed using equation 4. The maximum likelihood method (MLM) is chosen for b-value estimation because it provides the least biased estimate (see Aki 1965). Chan and Chandler (2001) and Amorese et al. (2010) in their work have opined that b-value needs to be calculated on a de-clustered catalogue. De-clustering means that dependent events like the foreshocks and aftershocks related to a major earthquake are to be removed from the catalogue. The b-value calculated on de-clustered catalogue is thus statistically unbiased and robust. In the present case, the b-value is calculated by MLM after the dataset is de-clustered using the procedure defined by Kafka and Walcott (1998).

The earthquake magnitude equal and above Mc are subjected to b-value calculation with error estimation in calculation by using equation 3 and 4 for four clusters and tabulated (Table 1). The b-value ranges from 0.78 in cluster III, 0.79 in cluster I, 0.95 in cluster II, to 1.11 in cluster IV. As the parameter 'b' acts as a 'stress-meter' in earth's crust and depends on the effective stress regime and tectonic character of the region (Hatzidimitriou et al. 1985; Tsapanos 1990), low 'b' within the clusters correlates with increasing effective stress levels prior to a major shock (Kanamori, 1981) or an increase in applied

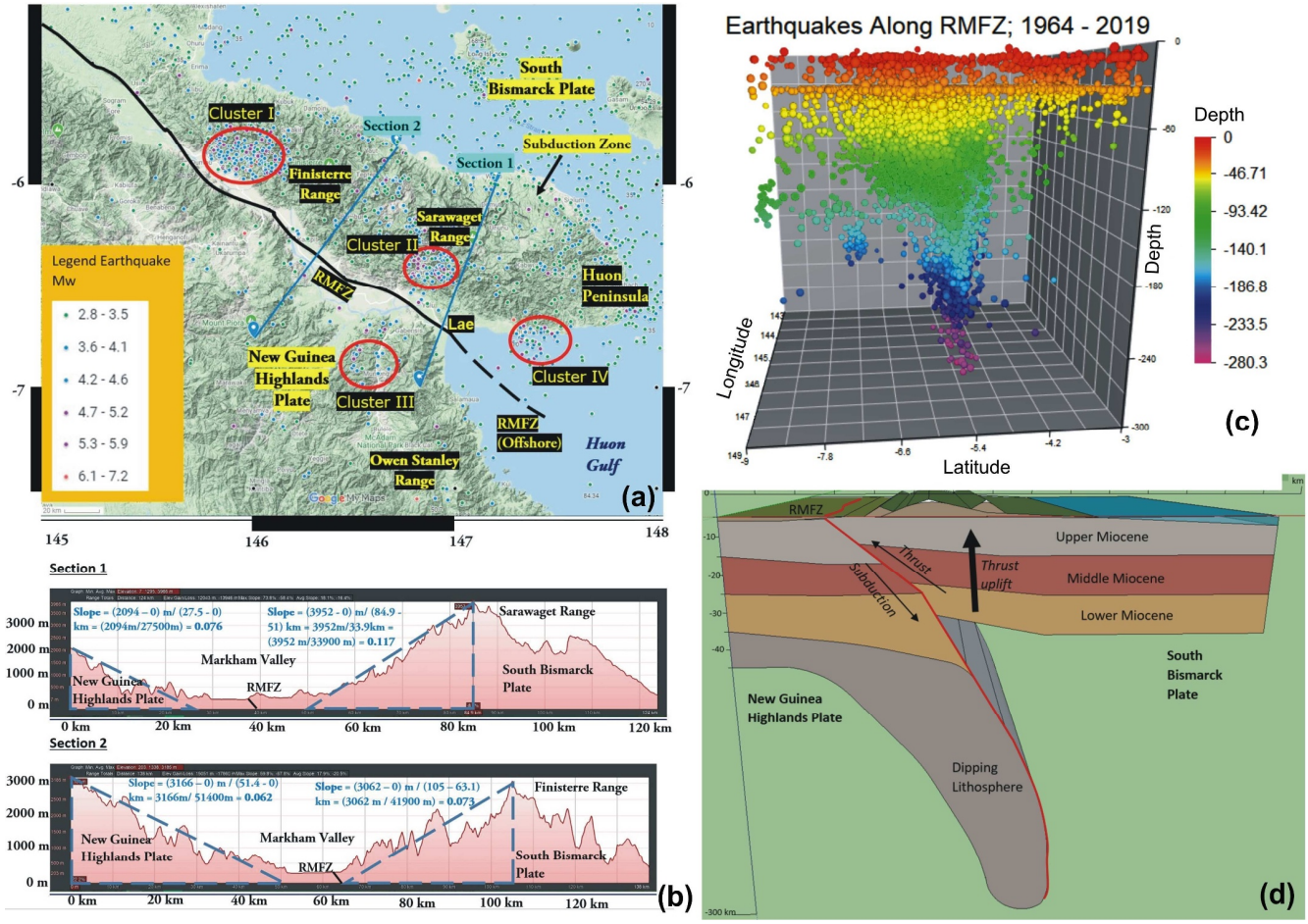

Fig. 3. **(a)** Seismicity clusters (I through IV) with magnitude variation, identified in close correspondence to RMFZ, located onshore and offshore, in eastern Papua New Guinea. The locations of two topographic sections (section 1 and 2) are marked. **(b)** The topographic sections (1 and 2) where the disposition of RMFZ in Markham valley and its relationship with two plates (New Guinea Highlands plate and South Bismarck Plate) which are forming highlands on both sides are marked. **(c)** 3D distribution of seismicity along the subducting plate where focal depth of earthquakes extends down to 280 km. **(d)** The geometry and disposition of subducting (New Guinea Highlands plate) and overriding (South Bismarck Plate) plates in relation to RMFZ and its overall surface manifestation is illustrated.

shear stress / effective stress in the region (Urbancic et al. 1992). Hence, the b-values calculated for all the clusters indicate high effective stress level.

The relationship between b-value and different style of faulting has been investigated by Schorlemmer et al. (2005) from global catalogue. Their observation is that b-value systematically changes with different styles of faulting. It indicates that normal faulting events shows highest b-values (~1.2); strike-slip events with intermediate values (~1.0) and thrust events exhibits the lowest values (~0.90). Following Schorlemmer et al. (2005), the low b-values in cluster I to III indicate the probability of occurrence of compressional earthquakes in those clusters, and comparative high b-value in cluster IV indicate the possibility of occurrence of earthquake generated by strike slip faulting.

SEISMIC HAZARD ANALYSIS FOR THE CLUSTERS

Expected Mw, Gumbel Type III Statistics and Surface Rupture Length

The expected seismic hazard in terms of magnitude (Mw) is calculated for all clusters by Gumbel type III extreme value statistics (Gumbel 1958) and from surface rupture length (SRL) using the formula (equation 5 & 6) given by Wells and Coppersmith (1994).

Gumbel type III extreme value statistics is performed using the methodology and equations given in Appendix I, where the largest observed magnitude (M_{max}) for successive 5 years (t) interval is extracted for time period (1974 – 2018) for each clusters (I to IV). The different M_{max} obtained for the time period are arranged in increasing order of magnitude, and then the rank is assigned (rank j = 1, 2, 3, …10). Subsequently, Pj is calculated for all intervals using the equations 7 given in Appendix I. M_{max} is plotted against Reduced Variate (RV), where RV = [– ln (- lnPj)]. The probability distribution between RV and M_{max} is fitted by a linear curve. The linear regression equation of the fitted curve for all the four clusters are presented on Figure 8. Considering return periods (T) as 25, 50 and 100 years, Reduced Variate (RV) is further calculated for the return periods (T). The maximum magnitude (M_{max}) that can be generated for each return period is calculated by regression equations given in Fig. 8 and also graphically. The results are tabulated (Table 2). From the plots and subsequent calculations, it is inferred that the maximum magnitude (M) earthquake that can occur within 100 years are 6.9, 6.7, 7.5 and 5.8 M in clusters I to IV respectively.

Wells and Coppersmith (1994) has proposed an empirical relationship between the expected surface rupture length (SRL) and the size of the earthquake (M), valid for reverse faulting in inter-plate tectonic region. The strike length for the respective cluster zones is measured on map (Fig. 3). The strike length actually mimics the maximum SRL that can be generated by an earthquake in that cluster.

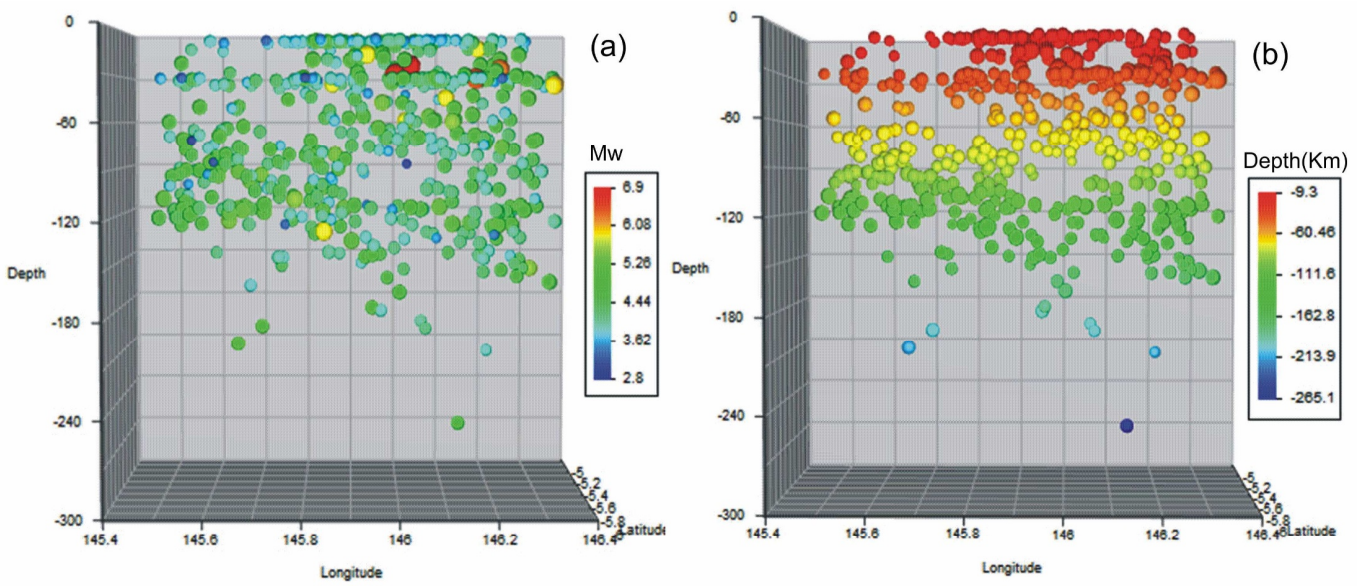

Fig.4. Seismicity in cluster I. **(a).** Distribution of Magnitude (Mw) with depth. **(b).** Seismicity coming from different focal depth range.

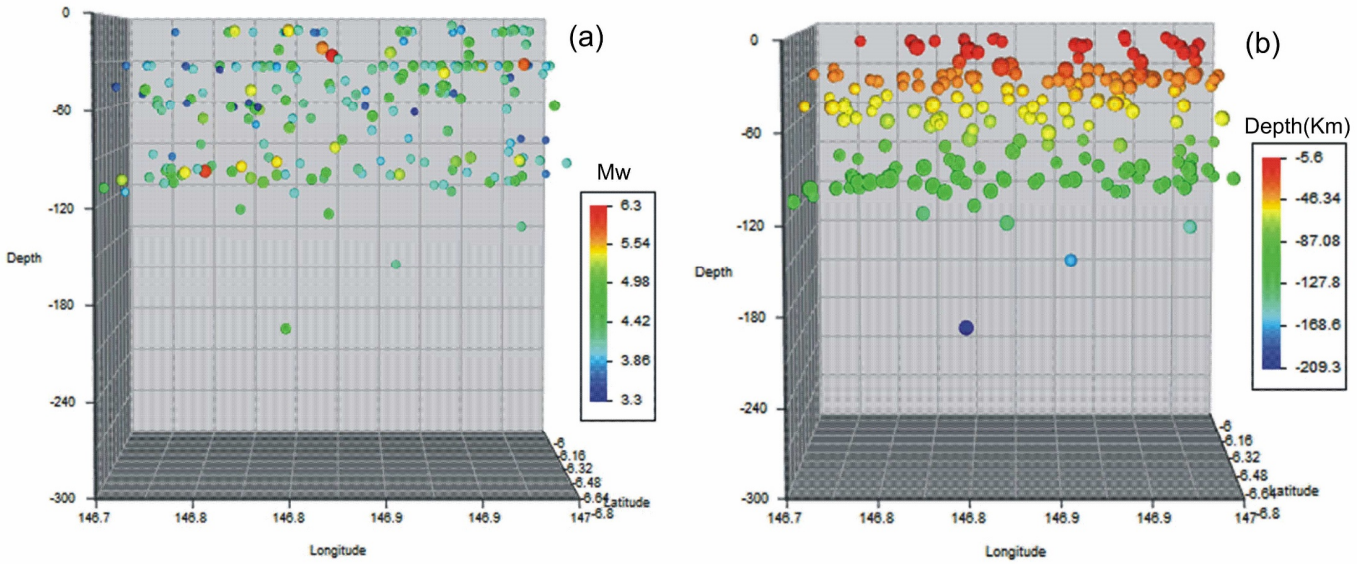

Fig.5. Seismicity in cluster II. **(a).** Distribution of Magnitude (Mw) with depth. **(b).** Seismicity coming from different focal depth range.

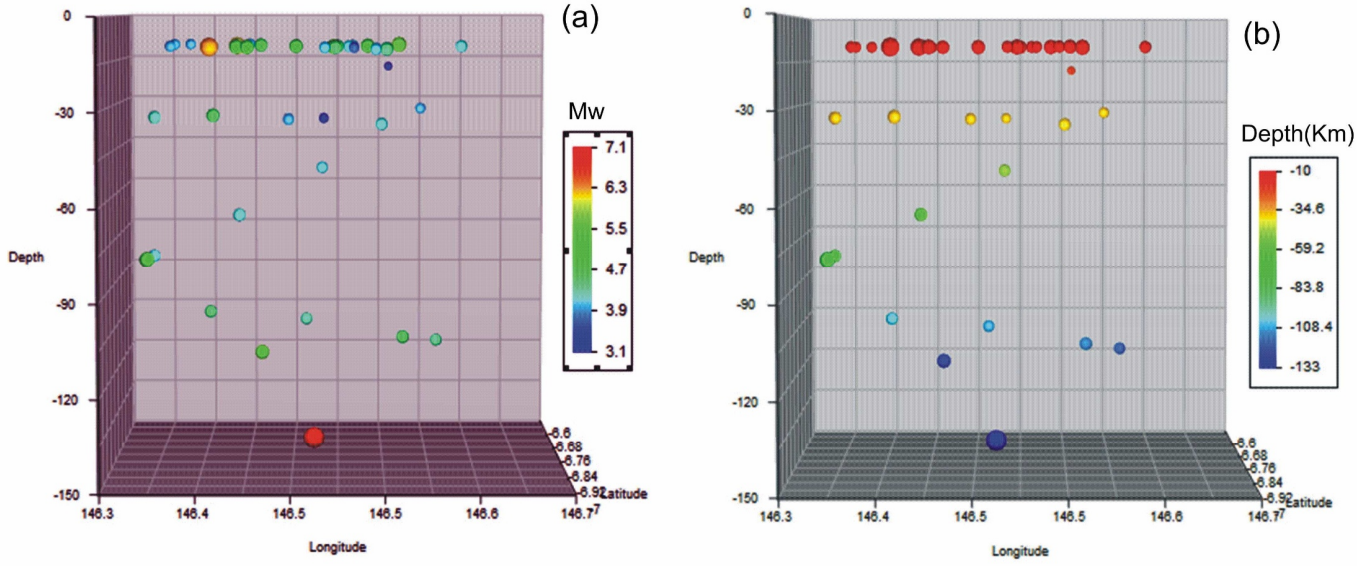

Fig.6. Seismicity in cluster III. **(a).** Distribution of Magnitude (Mw) with depth. **(b).** Seismicity coming from different focal depth range.

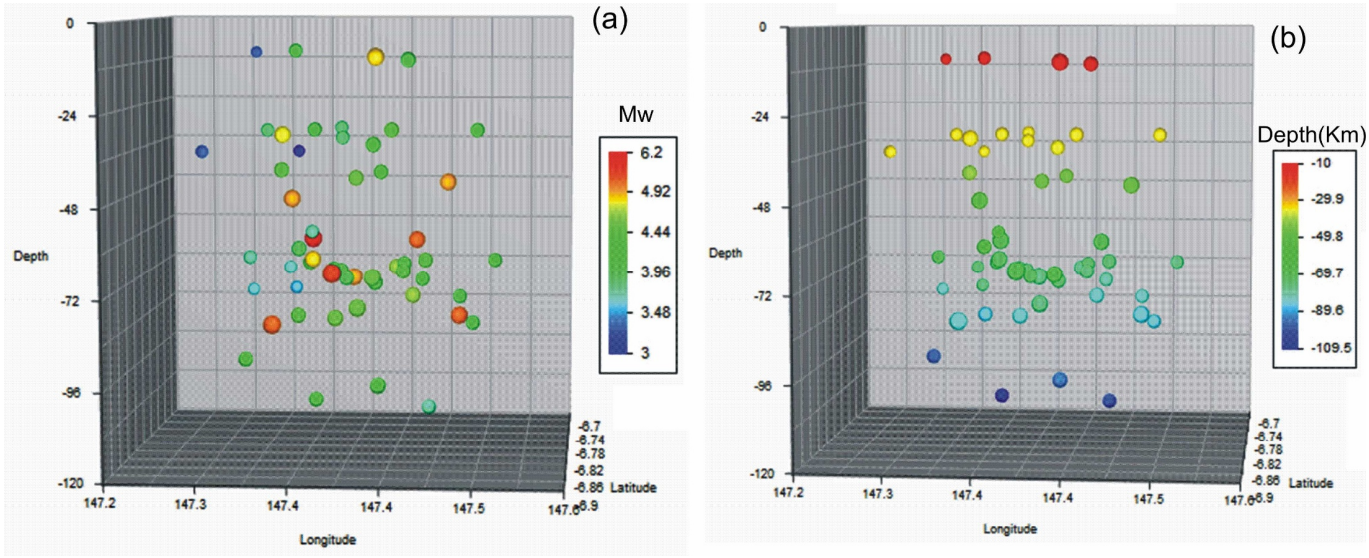

Fig.7. Seismicity in cluster IV. **(a)**. Distribution of Magnitude (Mw) with depth. **(b)**. Seismicity coming from different focal depth range.

Once the SRL is measured, the expected size of an earthquake is empirically calculated using the equation 5. The estimates are in Table 3 which shows a magnitude range between 7.0 and 7.3. The estimated magnitude is in higher order than actually observed, presuming that the length of the cluster is ruptured in a single instance. But in reality, smaller SRL is also expected which can give smaller magnitude earthquake. After calculating M, maximum displacement (MD) is calculated by equation 6. The range of slip displacement (Table 3) varies from minimum 4.08 metre for cluster II to maximum 6.45 metre for cluster I.

Temporal Clustering of Earthquake Moments within the Clusters

The earthquake moments in a seismic cluster is temporarily clustered. The temporal clustering is manifested by alternate clustering of high and moderate - low seismic moment values within short period of time in an earthquake catalogue. Such temporal clustering in moment data is best constrained by Hurst plot and Hurst coefficient developed by Hurst (1951, 1956) while working on the reservoirs of river Nile in Egypt. Hurst has developed a relationship, $R/S \sim N^h$ where R is the maximum range of cumulative departure from mean annual discharge of river, N is the year of observations, S is the standard deviation of river discharge and 'h' is a coefficient. The coefficient h is further approximated by another scalar K by Hurst (1951, 1956), where K is log(R/S)/log(N/2) and N is the number of samples. Any natural phenomena with temporal clustering shows K value greater than 0.5 (Wallis and Matalas, 1971). K value between 0 and 0.5 is indicative of anti-persistent behaviour in the dataset, while K between 0.5 and 1.0 indicates persistent behaviour with existence of temporal clustering in the dataset (Mansukhani, 2012).

For calculating coefficient K for N number of observations, the seismic moment values of successive earthquakes in each clusters are transformed logarithmically with base 10. Mean (M) and standard deviation (S) of the log transformed moment data are then calculated. From each moment data in the catalogue, the mean (M) is subtracted to get the values indicating difference from the mean. The cumulative departure from the mean is then computed by adding the values top to bottom in the catalogue. The cumulative departure from mean is plotted against sequential number of the event / year to generate the Hurst plot. Subsequently, range (R) is computed from the difference between the maximum and the minimum value of the cumulative deviation in

Table 1. Seismic parameters estimated for the Clusters I through IV.

Cluster	Total no of earthquake in the zone	Range in magnitude (Mw)	Major Shocks observed in the clusters	Magnitude completeness(Mc) by assumption of self-similarity (Wiemer and Wyss 2000)	b-value (Maximum likelihood method of Aki 1965) with error by Shi and Bolt (1982)
I	185	2.8 - 6.9	13.10.1993, Mw 6.9, 25.3 km depth 13.10.1993, Mw 6.5, 33 km depth 16.10.1993, Mw 6.2, 32.9 km depth 25.10.1993, Mw 6.7, 30.4 km depth 25.10.1993, Mw 6.1., 26.5 km depth	4.0	0.798 ± 0.072
II	117	3.4 – 6.3	29.10.1977, Mw 6.1, 110.5 km depth 05.11.1991, Mw 6.2, 82 km depth 06.04.1999, Mw 6.3, 17Km depth 04.06.2005, Mw 6.1, 28 km depth	4.2	0.951 ± 0.109
III	38	3.1 – 7.2	25.04.1974, Mw 7.2, 74Km depth. 05.05.2001, Mw 6.4, 15 km depth 06.05.2019, Mw 7.1, Bulolo Earthquake, Papua New Guinea, 146 km depth.	4.1	0.786 ± 0.176
IV	55	3.0 – 6.2	12.02.1986, Mw 5.7, 22.8 km· 17.04.2010, Mw 6.2, depth 62.9 km	4.1	1.119 ± 0.174

Table 2. Expected Maximum Magnitude (Mw) by Type III Gumbel Statistics with Return period (T) of 25 to 100 years for the Seismic Clusters I through IV.

Clusters	Return Period (T) in Years		
	25 years	50 years	100 years
I	5.9 M	6.4 M	6.9 M
II	5.8 M	6.2 M	6.7 M
III	5.8 M	6.6 M	7.5 M
IV	5.3 M	5.5 M	5.8 M

Table 3. Expected maximum magnitude and displacement in the four cluster zones, I to IV, calculated from Surface Rupture Length by using the approach given by Wells and Coppersmith (1994).

Clusters	SRL (km)	Magnitude expected(Mw)	Maximum displacement (m)
I	80	7.3	6.45
II	60	7.1	4.08
III	65	7.2	4.64
IV	50	7.0	3.07

the Hurst plot, and K is calculated by the formula $\log_{10}(R/S) / \log_{10}(N/2)$, where N is the total number of earthquake in the catalogue. The Hurst plot indicates the moment release pattern and its clustering.

The Hurst coefficient K is greater than 0.5 for all four clusters: cluster I: 0.674; II: 0.642; III: 0.628 and IV: 0.612 respectively. K-values indicates persistent behaviour in the earthquake catalogues and presence of temporal clustering of moments in the datasets. In the present case, the Hurst plots contain two distinct trends; positive and negative sloping moment release segments, sometimes forming a wave like pattern.

The Hurst plot for cluster I (Fig. 9a) illustrates the presence of one positive (between 21.05.1976 and 25.10.1993) and a corresponding negative slope-moment release segment (between 26.10.1993 and middle of 2019). The positive sloping moment release segment (indicate as 1) yields five major earthquakes in this cluster (13.10.1993, Mw 6.9; 13.10.1993, Mw 6.5; 16.10.1993, Mw 6.2; 25.10.1993, Mw 6.7; and 25.10.1993, Mw 6.1) with b-value 0.76±0.06. This is followed by a lengthy negative sloping moment release segment (indicates as 2) from 26.10.1993 to middle of 2019 with no major shock yielding a relatively higher b-value of 0.86±0.04.

The Hurst plot of cluster II (Fig. 9b) shows wave like alternate positive and negative sloping moment release segments. The plot starts with a positive segment (between 25.09.1974 and 05.11.1991; yielded a major shock of 6.2, b-value 0.63±0.14), followed by a negative segment (between 06.11.1991 and 04.06.1999, b value 0.70±0.16), then by a positive segment (between 05.06.1999 and 04.06.2005 with a major shock of 6.3 and another 6.1 at its end, b value 0.60±0.11), a corresponding negative segment (between 05.06.2005 and 22.09.2011, b-value 0.56±0.09) and finally ended with a positive sloping segment with a moderate shock of 5.4 (from 23.09.2011 to continuing presently, b-value 0.70±0.19).

The Hurst plot of cluster III (Fig. 9c) shows one positive (between 25.04.1974 and 05.05.2001, b-value 0.71±0.19) and a corresponding negative moment release segment (from 06.05.2001 to 24.10.2018, b-value 0.78±0.16) in moment release pattern. The positive sloping moment release segment starts with a major shock of 7.2 (25.04.1974) and ended with a shock of 6.4; the negative slope ends with another big earthquake 06.05.2019 (Mw 7.1) Bulolo Earthquake to initiate a probable positive sloping segment in future.

The Hurst plot of cluster IV (Fig.9d) shows three segments, starting with positive moment release segment with a moderate shock of 5.2 and ends with another one with Mw 5.7 (between 04.11.1977 and 12.02.1986, b-value 0.63±0.16), corresponding negative sloping segment (between 18.02.1986 and 14.09.2010, b-value 1.26±0.26), and finally followed by a positive sloping moment release segments starts with a moderate shock of 6.2 (17.04.2010) and continuing today with b-value 0.91±0.32.

The positive moment release segment is characterised by

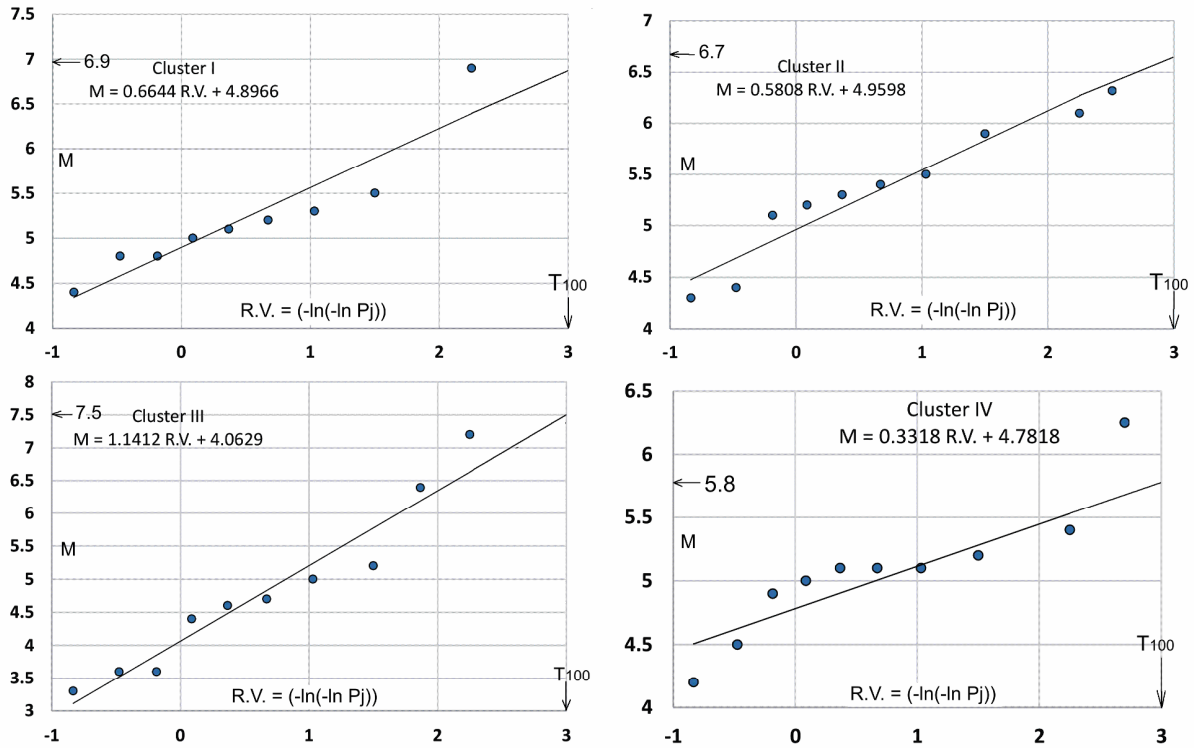

Fig.8. Estimated Maximum Magnitude and its probability through Gumbel's extreme value statistics for the Seismic Clusters I through IV in NE Papua New Guinea, for a return period of 25, 50 and 100 years. The best fit regression equations are also given in the diagram.

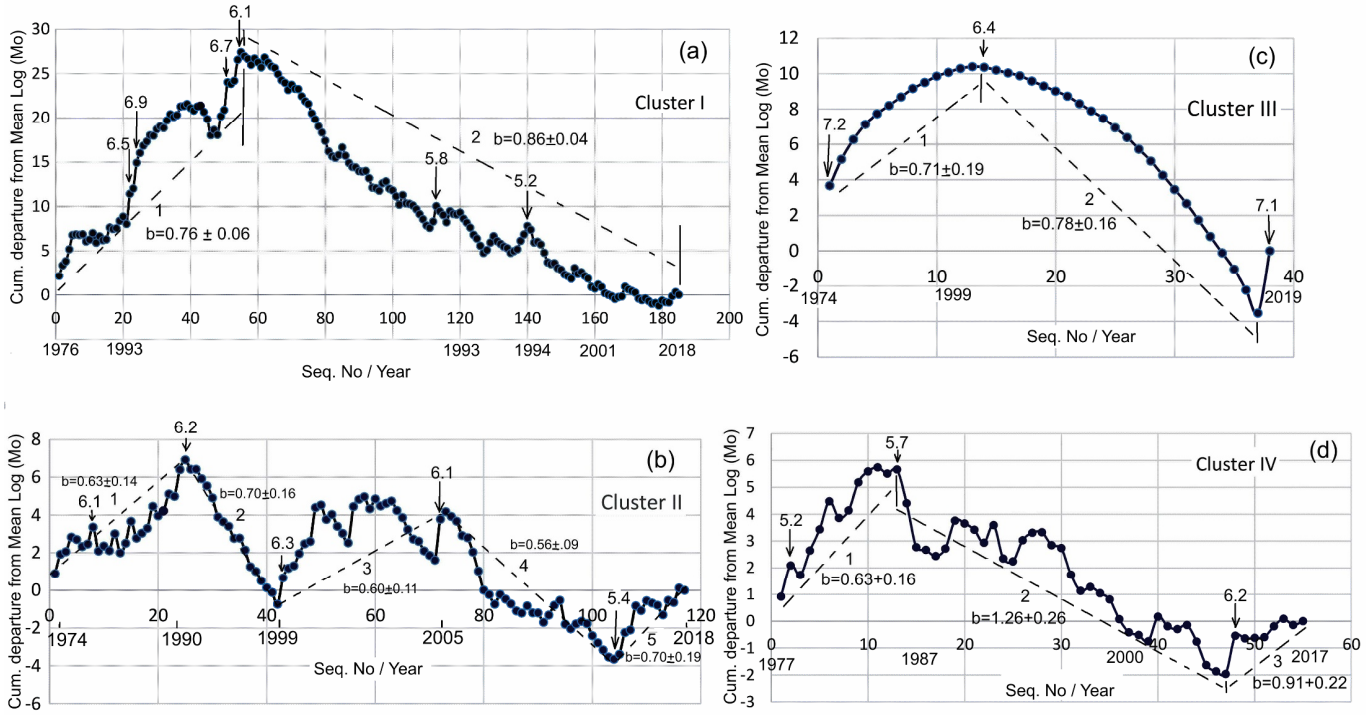

Fig. 9. Hurst plot of years against cumulative difference from mean Log cumulative moment release data of earthquakes of Cluster zones (I to IV). Plot indicates temporal clustering and manifested in the plot by alternate positive sloping (Clustering of large magnitude earthquakes/ seismic moments) and negative sloping (Clustering of small magnitude earthquakes/seismic moments) moment release segments indicating temporal clustering pattern with corresponding b-value. Hurst plot of **(a)** Cluster I, **(b)** Cluster II, **(c)** Cluster III and **(d)** Cluster IV.

accelerated moment release within a short span of time and thus indicating temporal clustering of larger magnitude earthquakes / seismic moments that exhibit lower b–value. The adjacent negative sloping seismic moment release segment however gives comparatively higher b-values. This phenomenon is observed in all plots described above. Low b – value is indicative of occurrence of bigger seismic events in comparison to smaller one, and point towards high seismic hazard. During the time of positive moment release, the smaller cracks that have been generated by earlier seismic cycle are joined together to form large cracks. In a progressive stress field, these large cracks are further joined with each other to form rupture by breaking the locked interface of the seismogenic fault to produce a large seismic event.

Paucity of large earthquakes in negative sloping moment release segment indicate decelerated moment release pattern or temporal respite in elastic strain release compared to the mean moment release rate in the catalogue. The temporal clustering of small magnitude earthquakes / seismic moments exhibits a comparatively higher b–value against the positive sloping segment. The b-value in this segment indicates clusters of smaller earthquake events and a phase of low seismic hazard. During this phase, numerous small cracks are formed.

The negative sloping moment release segment in a Hurst plot is important to access the timing of an impending large seismic event in a cluster. A prolong negative sloping moment release segment indicates interseismic elastic stress build-up and strain hardening. As per 'Elastic failure model' of Main et al. (1989), this strain hardening phase is followed by a short period of strain softening phase and dynamic failure to generate an earthquake with aftershock sequence as a part of seismic cycle. It proves further tenable for cluster III which produced the Bulolo earthquake of Mw 7.1 in 2019 at the end of a prolonged negative slope-moment release segment (Fig. 9c). Similar situation is also present in Cluster I which yields a persistent negative moment release segment from 26.10.1993 to till date. It is therefore inferred that the zone is likely to rebound back with a major earthquake of projected magnitude as big as Mw 6.9 (refer Table 2) at any point of time.

STRESS PATTERN IN SEISMIC CLUSTERS AND ITS VARIATION IN RESPECT OF THE RAMU-MARKHAM FAULT ZONE (RMFZ)

Seismic clusters I, II and IV which are present north of RMFZ along its dip direction are seemingly associated with the tectonic activities on its fault plane. If the fault geometry is followed, the earthquakes in cluster III which are occurring south of RMFZ illustrate no apparent relationship with the fault. To understand the nature of activities on both sides of RMFZ, stress analysis through the inversion

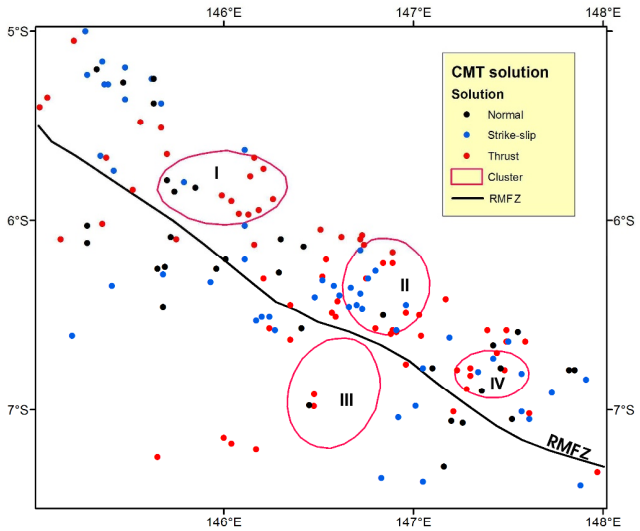

Fig. 10. The distribution of CMT data (Mw ≥ 5.0) with fault plane solutions on either side of RMFZ in the study area. Four spatial clusters (I to IV) are also shown.

of CMT data has undertaken, as discussed below.

The centroid moment tensor (CMT) focal mechanisms data for earthquakes having magnitude Mw ≥ 5.0 (source: http://www.globalcmt.org) in the study area around a buffer zone of 60 km north and south of RMFZ is plotted with designated fault pattern (thrust, strike slip and normal) deduced as per Aki-Richards convention on slip (Fig.10). The CMT data are further segregated into northern and southern areas depending on its location with respect to RMFZ.

Nature of tectonic stress is thus analysed through the inversion of these CMT data by using a computer programme "Win-Tensor", developed by Delvaux and Sperner (2003). Through this inversion, the orientations of the major stress axes (σ_1, σ_2 & σ_3), the stress ratio R [where $R = (\sigma_2 - \sigma_1) / (\sigma_3 - \sigma_1)$] and stress regime index R' are calculated to have a fair idea on the operative stress regime. At places, where extensional stress prevails (σ_1 is vertical), R' = R; but when it changes to compressional (σ_3 is vertical), R' = (2 + R). Accordingly, the stress pattern is analysed for the northern and southern territories bounding the RMFZ as compressive (thrust and strike-slip) or extensional (normal), experienced by the earthquakes. The local stress pattern is also analysed for four earthquake clusters (I to IV), three of which are detected below the northern area while one to the south of RMFZ.

RMFZ being a fault developed in the hinterland of a subduction zone, earthquakes typically experiencing the compressive stress are analysed further to obtain an idea on the regional stress pattern. The regional compressive stress pattern for the territory north of RMFZ is viewed next together with the variation in localised compressive stress for the clusters I, II and IV. Results for the northern territory exhibit a

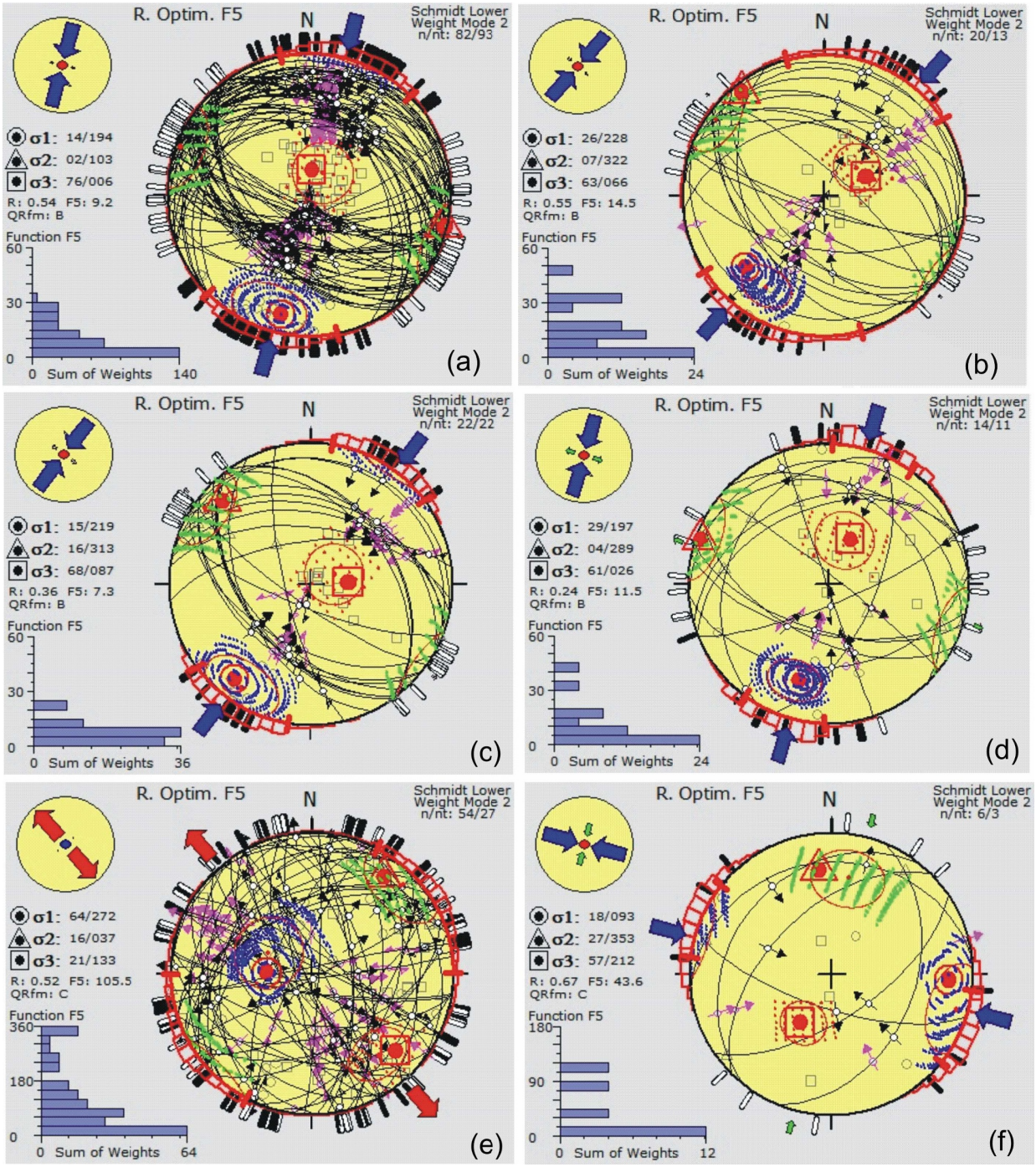

Fig.11. Compressive stress pattern as analysed from inversion of CMT data using Win-Tensor program developed by Delvaux and Sperner (2003). **(a)** Northern block of RMFZ, **(b)** Cluster I, **(c)** Cluster II, **(d)** Cluster IV, **(e)** Southern block of RMFZ, and **(f)** Cluster III.

Table 4. Table shows Stress Ratio (R) and Stress Regime Index (R') values for different tectonic domains along RMFZ, calculated from inversion of CMT data by Win-Tensor program of Delvaux and Sperner (2003).

Domains	Stress Ratio (R)	Stress Regime Index (R')
Northern Block of RMF: Compressive Stress earthquakes	0.54	2.54
Northern Block of RMF: Extensional Stress earthquakes	0.39	0.39
Southern Block of RMF: Compressive Stress earthquakes	0.52	2.52
Southern Block of RMF: Extensional Stress earthquakes	0.65	0.65
Cluster I	0.55	2.55
Cluster II	0.36	2.36
Cluster III	0.67	2.67
Cluster IV	0.24	2.24

consistent compressive stress pattern in both regional and local scales; the stress regime index R' being 2.54 (Table 4). Regional compressive stress for the northern territory is thus envisaged to represent a 'pure compressive' stress regime, where σ_3 is almost vertical and σ_1 is horizontal (Fig. 11a). Orientation of major stress axes (Figures 11 b, c, d) for three of the localised clusters (I, II, and IV) belonging to the northern territory thus agrees with that deduced from the regional stress pattern. The value of R' changes from 2.55 to 2.24 through 2.36 for the clusters I, II and IV (Table 4), suggesting thereby that the local stress regime undergoes a gradual change from 'pure compressive' to 'pure transpressive' across the RMFZ.

The Win-tensor denotes the stress regime for southern areas of RMFZ (Fig.11e) as an extensional one in spite of analysing the CMT data for the compressive earthquakes only. This is because the compressive stress pattern for southern areas of RMFZ does not follow any particular pattern, this is further documented by the rose diagrams that are created from the strike directions of causative fault planes for compressive earthquakes (Figs. 12 a, b). The fault planes are dominantly NW-SE to the north of RMFZ (Fig.12a) but clearly lost orientations south of RMFZ (Fig.12b). This we visualize to be an outcome of two different mechanisms: (i) either the effect of the Bismarck Sea subduction is no longer persists south of RMFZ, or (ii) there are free-moving detached slabs (namely; cluster III), as relics of the past subduction, from the presently advancing plate.

Earthquakes for cluster III exhibit a 'pure compressive' stress regime (Fig. 11f) almost tending to be a 'radial compressive' as observed from the stress regime index R' (Table 4). However, in cluster III, the orientations of the major stress axes (σ_1, σ_2 & σ_3) do not coincide with that for the regional or local stress pattern envisaged for northern areas (Figs. 11 a through d).

DISCUSSION

As a part of seismic hazard analysis in clusters, the probable earthquake size and nature of which are analysed and tabulated in Table 1 to 3. The b-value 0.786 (cluster III), 0.798 (cluster I), 0.951 (cluster II) to 1.119 (cluster IV)) indicates high stress domains with probability of occurrence of megathrust earthquakes in those clusters. The size of seismic hazard calculated by extreme value Gumbel statistics with a return period of 100 years is 6.9, 6.7, 7.5 and 5.8 M in clusters I to IV respectively. Cluster I has generated five large thrust earthquakes of Mw 6.1 to 6.9 in October 1993 at shallow focal depth beneath the Finisterre range, whereas, detached slab (?) at greater depth beneath cluster III has produced the 06.05.2019 Bulolo earthquake of Mw 7.1, h = 146 km.

The Hurst coefficient K for all the clusters is above 0.5 indicating presence of temporal clustering within the clusters. This is illustrated in Hurst plots of all the clusters, which contains distinct trends; positive and negative sloping moment release pattern forming a wave like form. The positive moment release segment is characterised by accelerated moment release with low b–value, whereas the negative sloping segment indicates slightly higher b-value. As per our analysis, the persistent negative moment release segment in recent times within Cluster I bears the capability to bounce back with a major event of Mw 6.9.

The stress pattern is analysed by Win-Tensor (Delvaux and Sperner 2003) through the inversion of CMT focal mechanism data for northern and southern territories of RMFZ, and also for four earthquake clusters (I to IV) on either side of RMFZ. From the stress analysis, it becomes apparent that the northern block of RMF shows a 'pure compressive' stress regime with stress regime index R' being 2.54. The Clusters I, II and IV present in the northern areas shows a change in stress regime from 'pure compressive' to 'pure transpressive' with R' value changes from 2.55 to 2.36 to 2.24 in the direction NW to SE along the RMFZ fault zone. This is significant because it indicates a probable clockwise rotation of the plate as indicated by analysis of GPS data (refer Wallace et al. 2004 for details). The changes in b-value of the clusters (0.79 in cluster I, to 0.95 in cluster II, and 1.11 in cluster IV) also support this gradual changes in the stress regime. In contrary, the southern block

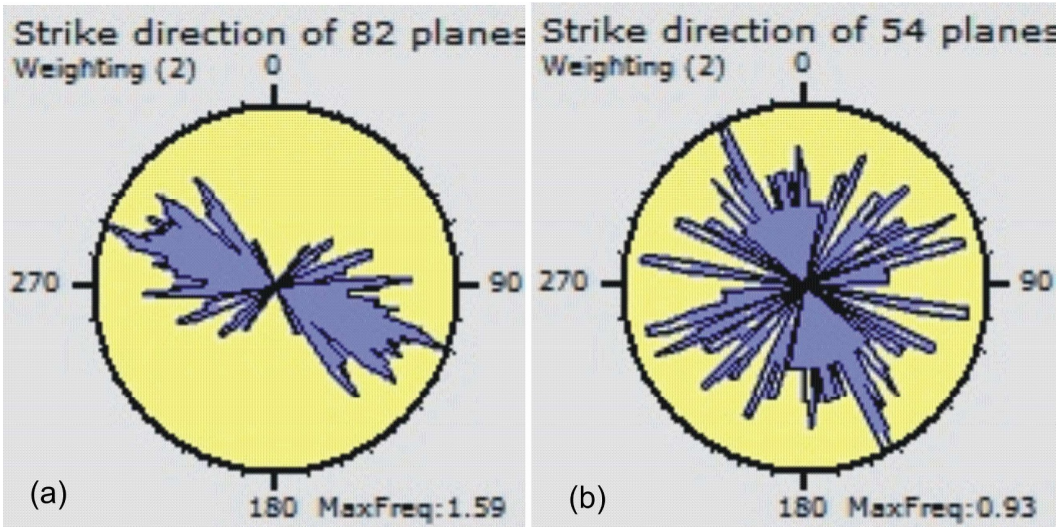

Fig.12. Rose diagram of strike direction of causative fault planes for compressive earthquakes, (a) Northern block of RMFZ where fault planes are dominantly NW-SE and (b) Southern block of RMFZ where fault planes are randomly oriented.

of RMF do not show any particular stress pattern and causative faults are almost haphazardly oriented indicating presence of a free moving floating disjointed slab detached from main subducting slab of NGH microplate in the shallow mantle.

CONCLUSIONS

The following major conclusions are arrived from the present study:

(a) Earthquakes in eastern PNG originate from four seismic clusters, within which, the focal depth extends to 240 – 300 km. RMFZ traverses the entire region in NW-SE direction over a distance exceeding 400 km through the Markham valley separating the PNG highlands within the study area, and for another considered distance of 100 km offshore past the port-city Lae. 3D-representation for all four Seismic clusters are presented and discussed.

(b) The close correspondence between the seismic clusters, the DEM and the fault disposition is indicative of detached lithospheric slabs in the hinterland of the ongoing subduction front located some 100 km further north of the RMF. It is thus visualized that the RMF is probably a deep penetrative steep angle tectonic divide, rather than a crustal ramp-fault as envisaged by Stevens et al. (1998).

(c) The spatial and temporal characteristics of magnitude Mw and moment (Mo) represented by the seismic clusters are studied by the following means: (i) b-value by MLM; (ii) expected magnitude, Mw, by Gumbel extreme value statistics and SRL; (iii) the temporal clustering of moments by Hurst Coefficient (K) and Hurst plot. The characteristics found for the seismic clusters are clearly representative of the rheological behaviour of the RMFZ; where clusters I, II, and IV are generated by the activity of RMFZ. However, cluster III is not related to RMFZ.

(d) The stress pattern for four earthquake clusters (I to IV) on either side of RMFZ and overall stress pattern in the hanging-wall (northern block) and foot-wall (southern block) of RMFZ are studied. The hanging wall part of RMFZ shows a 'pure compressive' stress regime. Where, the clusters I, II and IV in the hanging-wall part of RMFZ shows 'pure compressive' to 'pure transgressive' stress regime with indication of a probable clockwise rotation of the plate interface. However, the footwall block (southern block) of RMFZ which also contains cluster III (the zone of the 06.05.2019 Bulolo earthquake, Mw 7.1) do not show any particular stress pattern where causative faults are randomly oriented. It indicates presence of a free moving detached lithospheric slab in the hinterland of the current subduction-front further north.

(e) It is expected that the seismic clusters in eastern PNG have their own implications for the surface environment and population, in particular, for higher magnitude earthquakes occurring at shallow depths. In fact, the cluster I is showing such trend which can generate an earthquake of Mw 6.9 in any point of time. An earthquake of comparable magnitude and focal-depth coming from cluster IV in offshore Lae will pose an additional threat for tsunami, which may affect the port city. Further seismic hazard analysis studies are thus warranted for the region.

References

Abers, G., and McCaffrey, R. (1988) Active deformation in the New Guinea fold and thrust belt: Seismological evidence for strike slip faulting and basement involved thrusting. Jour. Geophys. Res., v.93, pp.13332–13354.

Aki, K. (1965) Maximum likelihood estimate of b in the formula log N = a-bM and its confidence limits. Bull. Earthquake Res. Inst., Tokyo Univ., v.43, pp.237-239.

Amorese, D., Grasso, J-R., and Rydelek, P.A., (2010) On varying b-values with depth: results from computer-intensive tests for Southern California. Geophys. Jour. Internat., v.180, pp.347–360.

Anton, L. and Gibson, G., (2007) Earthquake hazard in Papua New Guinea: Problems and the way forward. Monash Univ., Melbourne. https://www.researchgate.net/profile/Gary_Gibson4/publication/237387648_Earthquake_Hazard_In_Papua_New_ Guinea_Problems_And_The_Way_Forward/links/552bbdbd0cf 29b22c9c1e0a0.pdf.

Chan, L.S. and Chandler, A. M. (2001) Spatial bias in b-value of the frequency magnitude relation for the Hong Kong region. Jour. Asian Earth Sci., v.20, pp.3–81.

Delvaux, D. and Sperner, B. (2003) Stress tensor inversion from fault kinematic indicators and focal mechanism data: the TENSOR program. *In:* Nieuwland D (Ed.), New Insights into Structural Interpretation and Modelling. Geol. Soc. London, Spec. Publ., v.212, pp.75-100.

Gumbel, E.J. (1958) Statistics of Extremes. Columbia Univ. Press, New York, 375p.

Hatzidimitriou, P., Mountrakis, D.P. and Papazachos, B. (1985) The seismic parameter b of the frequency-magnitude relation and its association with the geological zones in the area of Greece. Tectonophysics, v.120, pp.141-151.

Hanks, H.C., and Kanamori, H., (1979) A moment magnitude scale. Jour. Geophys. Res., v.84(B5), pp.2348-2350. DOI: 10.1029/JB084iB05p02348.

Hayes, G. and Crone, T. (2019) At what depth do earthquakes occur? What is the significance of the depth? section in Natural Hazards. Retrieved from United States Geological Survey. https://www.usgs.gov/faqs/what-depth-do-earthquakes-occur-what-significance-depth?qt-news_science_products=0#qt-news_science_products.

Hurst, H.E. (1951) Long term storage capacity of reservoirs. T. Amer. Soc. Civil Eng., v.16, pp.770-808.

Hurst, H.E. (1956) Methods of using long-term storage in reservoirs. Proc. Inst. Civil Eng. Part 1, 5, pp.519-590.

Kanamori, H. (1981) The nature of seismic patterns before large earthquakes. *In:* Simpson, D.W., and Richards, P.G. (Eds.), Earthquake Prediction: An International Review, Maurice Ewing Series, Vol.4, AGU, Washington D.C., pp.1-19.

Main, I.G., Meredith, P., and Jones, C. (1989) A reinterpretation of the precursory seismic b-value anomaly from fracture mechanics. Geophys. Jour. Internat., v. 96, pp.131–138.

Mansukhani, S. (2012) The Hurst Exponent: Predictability of Time Series. Analytics Magazine, Issue July/August 2012, http://analytics-magazine.org/the-hurst-exponent-predictability-of-time-series/

Mcguire, R.K. (2004) Seismic Hazard and Risk Analysis, EERI Monograph 10, Earthquake Engineering Research Institute, Oakland, California, 221p.

Mukhopadhyay, B., Sengupta, D., Mondal, P. K., and Gonnade, G.D. (2016) Seismotectonic appraisal and tsunami potentiality of the seismic source zones in Andaman-Sumatra arc system, Indian Ocean. Indian Jour. Geosci., v.70, pp.139-152.

Schorlemmer, D., Wiemer, S. and Wyss, M. (2005) Variations in earthquake-size distribution across different stress regimes. Nature, v.437, pp.539-542.

Scordilis, E.M. (2006) Empirical global relations converting MS and mb to moment magnitude. Jour. Seismol., v.10, pp.225–236.

Shi, Y. and Bolt, B. A. (1982) The standard error of the magnitude-frequency b-value. Bull. Seismo. Soc. Amer., v.721, pp.1677–1687.

Stevens, C., McCaffrey, R., Silver, E.A., Sombo, Z., English, P., van der Kevie, J. (1998) Mid crustal detachment and ramp faulting in the Markham Valley, Papua New Guinea. Geology, v.26, pp.847– 850.

Stanaway, R. (2014) Deformation modelling to support the Papua New Guinean Geodetic Datum 1994 (PNG94). Kuala Lumpur, FIG Congress.

Stanaway, R., Wallace, L., Sombo, Z., Peter, J., Palusi, T., Safomea, B., and Nathan, J., (2009) Lae, a city caught between two plates – 15 years of deformation measurements with GPS. 43rd Association of Surveyors PNG Congress, Lae, 12th - 15th August 2009, Focus on Challenges; Society-Space-Surveyors.

Tregoning, P., Lambeck, K., Stoltz, A., Morgan, P., McClusky, S. C., Van der Beek, P., McQueen, H., Jackson, R.J., Little, R.P., Laing, A., and Murphy, B., (1998) Estimation of current plate motions in Papua New Guinea from Global Positioning System observations. Jour. Geophys. Res., v.103, pp.12181-12203.

Tregoning, P., Jackson, R. J., McQueen, H., Lambeck, K., Stevens, C., Little, R. P., Curley, R., and Rosa, R. (1999) Motion of the South Bismarck Plate, Papua New Guinea. Geophys. Res. Lett., v.26, pp.3517–3520.

Tsapanos, T. (1990) b-value of two tectonic parts in the circum-Pacific belt. PAGEOPH, v. 143, pp.229-242.

Urbancic, T.I., Trifu, C.I., Long, J.M., and Young, R.P. (1992) Space-time correlation of b values with stress release. PAGEOPH, v.139, pp.449-462.

Wallace, L. (2002) Tectonics and arc-continent collision in Papua New Guinea: Insights from geodetic, geophysical and geologic data. PhD Thesis, University of California, Santa Cruz, 244p.

Wallace, L.M., Stevens, C., Silver, A., McCaffrey, R., Loratung, W., Hasiata, S., Stanaway, R., Curley, R., Rosa, R., and Taugaloidi, J. (2004) GPS and seismological constraints on active tectonics and arc continent collision in Papua New Guinea: Implications for mechanics of microplate rotations in a plate boundary zone. Journal of Geophysical Research: Solid Earth 109, pp.B5. DOI: 10.1029/2003JB002481

Wallis, J.R., and Matalas, N.C. (1971) Correlogram analysis revisited. Water Resour. Res., v.7, pp. 448-1459. DOI: 10.1029/WR007i006p01448.

Wells, D.L., and Coppersmith, K.J. (1994) New empirical relationships among magnitude, rupture length, rupture width, rupture area and surface displacement. Bull. Seismol. Soc. Amer., v.84(4), pp.974-1002.

Wiemer, S. and Wyss, M. (1997) Mapping the frequency-magnitude distribution with depth in two volcanic areas: Mount St. Helens, Washington, and Mount Spurr, Alaska. Geophy. Res. Lett., v.24, pp.189-192.

(Received: 20 September 2019; Revised form accepted: 19 September 2020)

Appendix 1

Theoretical formulation for the calculation of Type III Gumbel extreme-value statistics (see also Mukhopadhyay et al. (2016)).

Gumbel (1958) has defined a stochastic process F(m,t) of a random variable 'm' on a time scale 't', and speculated 'M' be the maximum magnitude that can occur within a given time interval. The variable 'M', the extreme value defines a regular point process is embedded in the original process F(m,t) and expressed by the equation;

$P [M \leq m] = P [N = 0] = \exp (-P(m)\ \alpha\ t)$ ——(1),

where α is the mean number of earthquakes per year above magnitude zero.
With probability $P(m) = 1 – F(m)$ and t = 1 year, equation 1 becomes

$P(m) = \exp [- \alpha (1 – F(m))]$——(2).

It is assumed that a homogeneous earthquake process with a cumulative probability density function represented the negative exponential distribution for large earthquakes (where β is a constant) is defined as

$F(m) = 1- \exp(-\beta m)$———(3).

Combining equations (2) and (3); we obtain

$P(m) = \exp [-\alpha \exp (-\beta m)]$ ——— (4).

Equation 4 is known as the "Gumbels Type I distribution of extremes" and can be rewritten as

$-\ln (P(m)) = \alpha \exp (-\beta m)$

or

$-\ln [- \ln (P(m))] = - \beta m - \ln \alpha$ —— (5).

The left hand expression in equation (5) is called the *Reduced Variate* 'RV' which has a special interest in Hazard studies using Gumbels Type III distribution.
This distribution considers an upper limit of extreme 'm' and can be expressed as

$P^{III}(m) = \exp [- \{(M-m)/(M-u)\}^q]$ ——— (6),

where 'M' is the upper limit of external 'M', q and u are parameters of the corresponding asymptotic distribution estimated by the method of least square.
We consider that M_1, M_2 …… M_n be the largest observed magnitude in a given region during N successive time interval, 't' (in years). The different M_{max} are arranged in increasing order of magnitude with rank j = 1, 2, …..N and

Pj (plotting position of j^{th} observation) = J / (N+1) —— (7),

where N is the number of equal time intervals.

The probability function can be traced on the Gambel extreme probability paper by plotting Mj = (j= 1,2,….n) versus plotting position Pj. For linear graph paper Mj is plotted against *Reduced Variate* RV, i.e. –ln(-lnPj) (see equation 5 above).

The mean return period of extremal M may be obtained for values equal to or exceeding M as,

$T \text{ (Return Period)} = (1 – Pj^{1/t})^{-1}$

and

$Pj = (1-1/T)^t$ ———— (8),

where 't' is reference time interval considered. This relation is used to derive the M_{max} for a given return period 'T'.